Materials Chemistry and Physics 173 (2016) 347–354

Contents lists available at ScienceDirect

Materials Chemistry and Physics

journal homepage: www.elsevier.com/locate/matchemphys

Optical and structural investigation of ZnO@ZnS core–shell nanostructures☆

Efracio Mamani Flores [a], Cristiane W. Raubach [a], Rogério Gouvea [a], Elson Longo [b], Sergio Cava [c], Mário L. Moreira [a, *, 1]

[a] CCAF, Instituto de Física e Matemática (IFM), Departamento de Física, Universidade Federal de Pelotas, Campus Capão do Leão PO Box 354, CEP: 96010970, Pelotas, RS, Brazil
[b] INCTMN-UNESP, Universidade Estadual Paulista, P.O. Box 355, Araraquara 14801-907, SP, Brazil
[c] CCAF, Centro de Desenvolvimento Tecnológico, Universidade Federal de Pelotas, Rua Félix da Cunha 809, Pelotas, RS, Brazil

HIGHLIGHTS

- Obtation of ZnO@ZnS decorated systens using different solvents by MAS methodology.
- Growth solvent dependence of hexagonal and cubic phases for ZnS.
- Potential application of ZnO@ZnS decorated nanostructures as replacement material for solar cells.
- Control over band alignment between ZnO and ZnS.

GRAPHICAL ABSTRACT

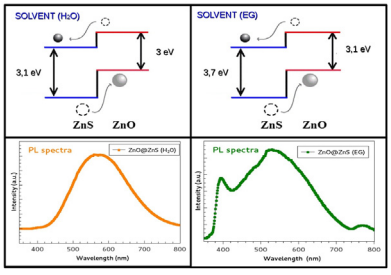

ARTICLE INFO

Article history:
Received 27 August 2015
Received in revised form
22 December 2015
Accepted 6 February 2016
Available online 12 February 2016

Keywords:
Photoluminescence spectroscopy
Semiconductors
Crystal structure
Optical properties
Crystal growth

ABSTRACT

In the present work, are reported the experimental study of ZnO@ZnS core–shell synthesised by a microwave-assisted solvothermal (MAS) method. Some synthesis parameters such as, time, precursor concentration and temperature were fixed. In order to investigate the effect of growing shell on the structural and optical properties, the samples were grown with two different solvent (water or ethylene glycol). The characterizations were performed by X-ray diffraction, absorption spectroscopy in the UV–vis range, scanning electron microscopy, and photoluminescence spectroscopy. The results show that both ZnO and ZnS diffractions are present for all samples, however the crystallinity degree of ZnS shell are too low. The better decorations of ZnS (shell) on the ZnO (core) are obtained for ethylene glycol (EG) solvent, which is verified through FE-SEM images of ZnO@ZnS (EG). On the other hand, non morphological solvent dependence was observed for ZnO multi-wires. Also the luminescent emission for decorated system in water were more intense and leads to form a type-II band alignment for ZnO@ZnS core–shell system.

1. Introduction

Oxide semiconductor with core–shell nanostructure presents great technological potential and has already been applied in many fields [1–3]. In the past decade the global research interest in wide band gap semiconductors has been focused on zinc oxide (ZnO) due

☆ This document is a collaborative effort.

* Corresponding author.
E-mail address: mlucio3001@gmail.com (M.L. Moreira).

[1] This is the specimen author footnote.

http://dx.doi.org/10.1016/j.matchemphys.2016.02.022
0254-0584/

to its excellent and unique properties as a semiconductor material. The high electron mobility, high thermal conductivity, good transparency, wide and direct band gap (3.1 eV–3.4 eV) and large exciton binding energy (60 meV) at room temperature [4] spread the potential applications of ZnO compounds. These properties make ZnO a promising material for optical devices such as laser diodes, light emitting diodes, solar cells, electroluminescent devices and ultraviolet laser diodes [5]. Unfortunately none of these important applications have not been well developed, then the scientific and technological investigations are still very important to help its ready development.

The photoluminescence (PL) spectrum of the ZnO exhibits two excitonic peaks [6], one in the UV region and other at visible region [7,8]. The broad emission band in the visible region (420 nm–750 nm) is attributed to deep level defects in ZnO [9,10]. There are many different deep level defects in the crystal structure of ZnO, such as, oxygen vacancy and short-range disorder, which can affect the optical and electrical properties of ZnO [11–13]. In this context, a remarkable number of research works aimed at improving the physical and chemical properties of ZnO by surface decorating or surface modification with another semiconductor [14,15]. A special case is the core–shell systems where shell plays an important role as a physical barrier between the optically active core and the surrounding medium [16–18].

ZnS belongs to II-VI semiconductor class with two possible crystal structures (zinc blend and wurtzite) and due to its wider band gap (3.65 eV) can be applied as a shell for ZnO nanostructures (NPs) [19]. The formation of ZnO@ZnS core–shell system, with lower band gap core(ZnO)/higher band gap shell(ZnS) structure can show different optical properties according to the band alignment [20,21], which has already been applied in solar cells, photocatalysis and water-splitting [22,23].

Recently, a wide variety of chemical techniques have demonstrated high efficiency to synthesize ZnO@ZnS core–shell systems, such as, co-precipitation, solgel, hydrothermal method and so on. Among these chemical techniques [24,25], the solvothermal process has attracted a great deal of attention since particles with the desired characteristics can be prepared with this technique by controlling the solution pH, reaction temperature, reaction time, solute concentration and solvent types, depending on the particular application [26]. The main advantages of solvothermal synthesis are related to homogeneous nucleation processes, ascribed to elimination of the calcinations step to produce very low grain sizes and high purity powders [27]. Besides the association of microwave radiation to solvothermal method generates a physical-chemical hydride synthesis methodology [28].

The present work aims at investigate the influence of solvent (EG or water) on the structural and optical properties of ZnO@ZnS core–shell system. For this purpose, ZnO@ZnS was prepared using the MAS method under water and EG mediums. The prepared particles were characterized by Thermogravimetry, X-ray diffraction (XRD), field-emission scanning electron microscopy (FE-SEM), Raman spectroscopy, ultraviolet–visible (UV–vis) spectroscopy and photoluminescence (PL) spectroscopy.

2. Experimental

2.1. Materials

The chemical reagents used were analytical grade without further purification and each synthesis were performed as follows description:

2.2. Synthesis of ZnO particles

ZnO nanorods were synthesized based on Moura et al. [29], the details are described as follows 2.6 mmol of zinc acetate dehydrate [$Zn(CH_3COO)_2.2H_2O$] were added to 80 mL of 1 mol. L^{-1} NaOH aqueous solution. After stirring 10 min. The resulting whitish aqueous solution was then transferred to a polytetrafluoroethene (PTFE), autoclave which was sealed and heated until 130 °C in 1 min and maintained at this temperature for 40 min in a microwave-assisted oven (2.45 Ghz, 800 W). The white solid precipitate product obtained was centrifuged and washed with distilled water-ethylene and finally dried at 60 °C in air.

2.3. Decoration of ZnO@ZnS core–shell system

The experimental procedure to decoration with ZnS was performed according to our recent work of Raubach et al. [30], previously synthesized ZnO powder (0.017 mol) was dispersed in 25 mL of EG or water generating solutions 1EG and 1W respectively. Then, 0.017 mol of Zinc acetate dehydrate [Zn $(CH_3COO)_2$ $2H_2O$] and 0.03 mol of thiourea were dissolved in 75 mL of EG or water generating solutions 2EG and 2W respectively. At this stage any surfactant was added. Solutions 1 and 2 were then mixed in a 120 mL polytetrafluoroethene and placed in the microwave system at 130 °C for 40 min. The resulting precipitates were washed several times with water and ethanol until a neutral ($pH \approx 7$) solution was obtained. Afterwards, the powders were collected and dried at 80 °C for 9 h in air, producing a straw white powder.

2.4. Characterization

The powder obtained were characterized by XRD data from 15° to 75° in the 2θ range using CuKα radiation (Rigaku-DMax/2500PC). Thermogravimetric analysis was performed using 5 °C/min of heating hate until 900 °C under air atmosphere. Microstructural characterization and EDS were performed on a field emission scanning electron microscope Carl Zeiss Supra 35-VP. Raman spectra were recorded in the range of 100–1000 cm^{-1} on a Bruker Equinox-55 (Germany) using the KBr pellet technique. UV–vis spectra were collected on a Agilent Cary 100 spectrophotometer in diffuse reflectance mode. The PL spectra were collected using a Thermal Jarrel-Ash Monospec monochromator and a Hamamatsu R446 photomultiplier. Krypton ion laser (Coherent Innova) with an exciting wavelength of 350.7 nm (2.57 eV) was used and the output of the laser was maintained at 200 mW. All measurements were taken at room temperature.

3. Results and discussion

3.1. Structural study

The crystallinity and crystal phases of the samples (ZnO, ZnS and ZnO@ZnS) synthesized at two different solvent (EG or water) were first examined by X-ray diffraction and the results are shown in Fig. 1. The diffraction peaks can be indexed of wurtzite (WZ) phase (ZW) for samples of ZnO synthesised in EG and water, indicating that formation of WZ phase of ZnO is not solvent dependent. For ZnS compound the zinc blende (ZB) phase was found for both solvents (EG and water), which is well consistent with the (JCPDS: 080-74 and 03-570) respectively. The samples ZnO@ZnS (water) are observed that ZW phase remained, and for ZnO@ZnS (EG) show a slight tendency to ZB phase due to peak broadening.

In the XRD spectra of ZnO (water) in (Fig. 1A) we can observe the formation of well crystalline hexagonal structure compared to ZnO (EG) shown in (Fig. 1B). This behaviour can be related to the high

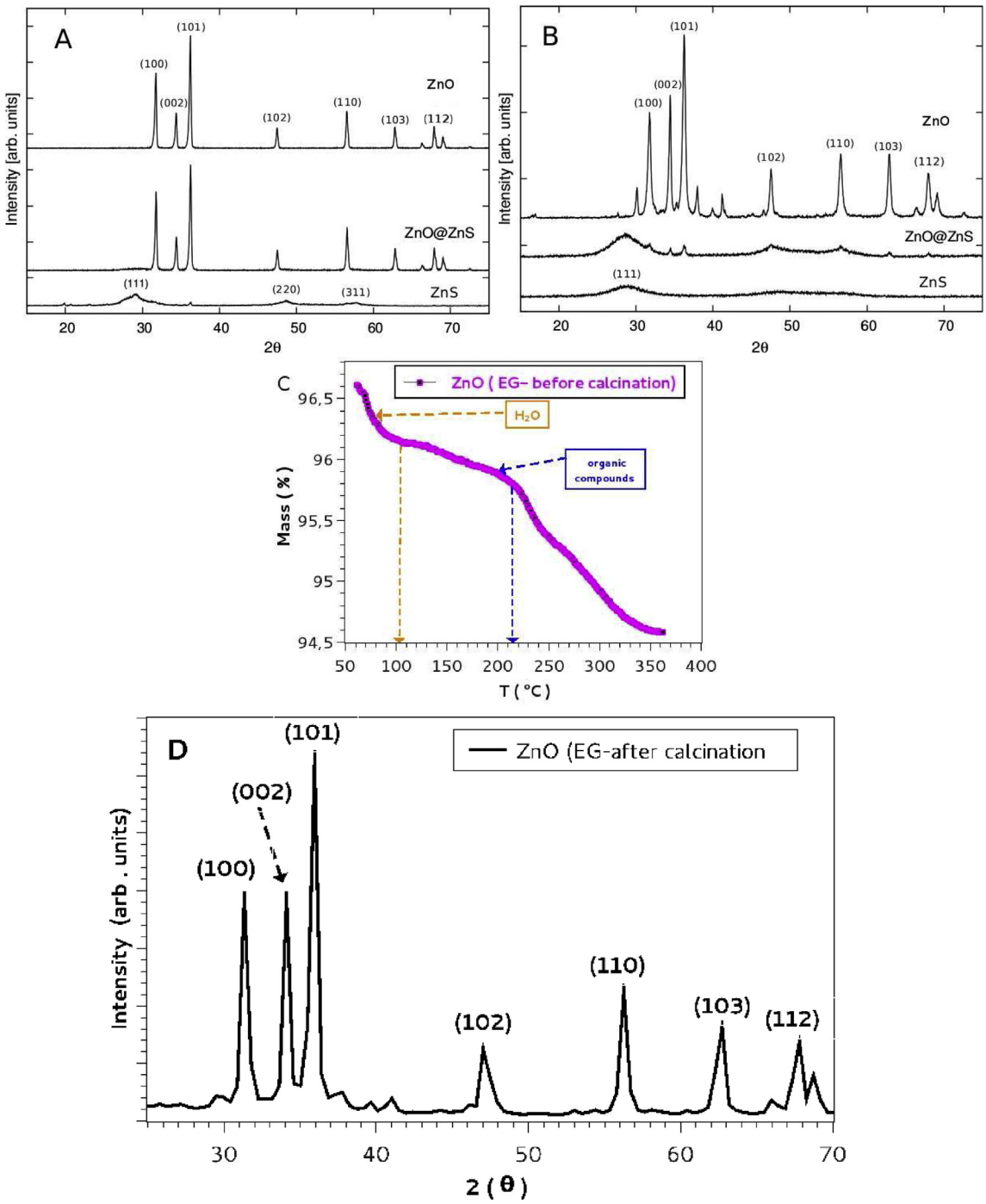

Fig. 1. XRD powder patterns of the ZnO and ZnO@ZnS core–shell synthesized in (A) shows the XRD of samples with solvent H_2O, (B) show the XRD of samples with solvent EG, (C) TGA curve of ZnO (EG) and (D) XRD of ZnO (EG-after calcination).

ion mobility in water them in EG, improving the effective collisions.

It can be seen that for the ZnO (EG) in (Fig. 1B) the diffraction peaks has a lower intensity compared with that of the ZnO (water) in (Fig. 1A), indicating a degradation of the crystalline structure of the ZnO when synthesized in EG. On the other hand XRD in (Fig. 1A) show that the ZnS (water) is single-phase compound. Notwithstanding for decorated system the crystal structure and orientation of ZnO (water) are preserved. However, when the samples are decorated with EG in (Fig. 1B) it should be noted that all peaks appear slight shifted to ZB phase and the peak intensity of ZnO (EG) is very weak compared to peaks of ZnO (water). Clearly is observed that the samples synthesized with solvent water, has a better crystalline quality and this is confirmed in FE-SEM images.

XRD spectra of a ZnO synthesized with EG solvent shown in Fig. 1B, highlights that the ZnO is not well crystallized as was obtained in water. This can be explained due to the nucleation process of ZnO was not completed, remaining a small amount as waste zinc hydroxide. The preferential orientation observed for peak (002) in (Fig. 1B) correspond to reinforcement diffractions of $Zn_5(OH)_6(CO_3)_2$ (JCPDS 19-1458, zinc hydroxide carbonate) [31] over ZnO

diffractions. After heating at 600 °C the $Zn_5(OH)_6(CO_3)_2$ was converted into ZnO. This process can be identified through sharp diffraction lines corresponding to well crystallized ZnO (JCPDS 080-74) (Fig. 1D), which are very similar XRD spectra before obtained for ZnO (water) and by intensity decrease of (002) peak in relation to (100) diffraction peak denoted in (Fig. 1D).

In Fig. 1C, show the thermogravimetric (TG) analysis carried out in the temperature range of 10°C–500 °C in an alumina crucible under air at 10 °C/min Fig. 1D, it shows the thermal behaviour (TG) of as-prepared compound obtained from direct precipitation of $[Zn(CH_3COO)_2.2H_2O]$, NaOH and EG and processed by MAS method. It can be seen that there are two pronounced mass loss steps, firstly in the temperature range 10°C–150 °C and followed by a range 160°C–400 °C, in TG curve. The first weight loss is mainly attributed to the evaporation of surface adsorbed water, whereas the second one might be ascribed to the volatilization and combustion of organic species in ZnO (EG). The first mass loss step was gradual and in the range of 10°C–150 °C. The mass loss was 2.4%, and this loss of mass is attributed to the removal of surface adsorbed water from aqueous urea and nitrate solution. The second step was the main weight loss occurred at 160°C-400 °C, and the loss was 2.8% which is due to the volatilization and combustible organic species present in the ZnO (EG). There is no associated signal with these latter thermal events in the TG curve, confirming no further crystallization and phase transition events of ZnO.

These results demonstrate that the use of solvent EG strongly influences the morphology and the growth preference of ZnO materials prepared by the solvothermal route. The EG favour the stabilization of zinc hydroxide acetate delaying ZnO phase formation and generate the lower crystallization degree.

3.2. Morphology study

The general morphologies of the samples synthesized by MAS method are shown in Fig. 2. In order to investigate the ZnO morphology, structures obtained at two different solvents (water or EG) were analysed by FE-SEM images as shown in Fig. 2a and c.

Fig. 2a shows the ZnO multi-wires under flower-like shape with 230 nm length and 100 nm width approximately. ZnO multi-wires present a smooth surface whereas ZnO (EG) exhibits a worm-like mesoporous surface (look top right corner) but also in a flower-like shape. Although the average diameter were not changed getting around 200 nm as measured from its FE-SEM image (Fig. 2c).

It has been observed that ZnS particles are spherical like regardless of solvent and also the particle size was not significantly changed.

The FE-SEM images of decorated samples (ZnO@ZnS) in water (Fig. 2b) and EG (Fig. 2d) show clearly that decoration in water medium is almost inefficient if compared to EG. Furthermore, the FE-SEM images of ZnO@ZnS (EG) shown in (Fig. 2e) that ZnO are well decorated with ZnS and to obtain further evidence the EDX spectrum was also performed. EDX qualitative analysis indicate that the zinc, oxygen and sulphur are present in the samples. This result can be used as another confirmation of decoration success.

3.3. Raman study

The Raman spectra of three samples synthesized with EG and water in a spectral range of 100 cm^{-1} to 700 cm^{-1} are shown in Fig. 3. The Raman spectroscopy is able to give further evidence for the crystallization, structural disorder and defects at short range order.

The ZnO wurtzite (WZ) structures belong to the $P6_3mc$ space group, with two formula units per primitive cell, where all atoms occupy (C_{6v}^4) sites. Group theory predicts the Raman active zone-centers of the optical phonons predicted to be $A_1 + E_1 + 2E_2$. The phonons having A_1 and E_1 symmetry are polar phonons and, hence, the transverse-optical (TO) and longitudinal-optical (LO) phonons exhibit different frequencies. Nonpolar phonon modes with symmetry E_2 have two frequencies: E_2 (high) is associated with oxygen atoms and E_2 (low) is associated with the Zn sublattice.

Fig. 3A. shows the corresponding Raman spectra for samples synthesized with water solvent. The decorated ZnO@ZnS obtained via water solvent almost preserves the same vibrations modes acquired for ZnO (water), indicating a poorly ZnS decoration. Three peaks of the as-obtained ZnO nanorods are observed at 346, 379 and 439 cm^{-1}, respectively. The main peak at 439 cm^{-1} is assigned to the E_2 (high frequency) optical phonon mode of ZnO (water), which corresponds to the band characteristic of a ZnO wurtzite [32]. Besides these classical Raman modes, weaker peaks at 346 cm^{-1} and 379 cm^{-1} can be assigned to A_1 (TO) and E_1 (TO) modes of ZnO, respectively. Thus, decorated ZnO@ZnS nanoforest was not affected by ZnS shell. This is a consequence of poor decoration and absence of active modes for zinc blend ZnS sample.

From Fig. 3B, show the confocal Raman scattering spectra of samples synthesized with EG solvent. The decorated ZnO@ZnS obtained via EG solvent which appears new vibration modes peaks due to the decoration of ZnS (EG). It is important to note that if the crystal is absolutely cubic, no active Raman modes are expected. Thus the observed vibrational modes for ZnS indicate that its cubic structure is not perfect and must be some structural localized defects. Nevertheless a weaker peak at 439 cm^{-1} is observed for ZnS sample and can be assigned to an E_2 optical phonon, which corresponds to characteristic band of WZ phase. Then pure ZnS (EG) or decorating ZnO in EG medium has a cubic phase, however there are a small fraction of hexagonal phase imperceptible to the X-ray diffraction. Main vibration observed at 439 cm^{-1} of as-obtained ZnO nanorods (water) was not evident for ZnO synthesized using EG, indicating a ZB tendency and/or a low crystallization process. The weak and broad peak at 251 cm^{-1} is assigned to the second-order Raman spectrum arising from the E_2 (high) E_2 (low) multiple phonons scattering process of ZnO@ZnS (EG). A comparison of the Raman spectra for the ZnO (EG) [33], shows an obvious shift in the E_2 (high) phonon mode of ZnO@ZnS (EG) to a low frequency. The peak width is broadened as a result of the decoration effect. For the wurtzite crystal structures, stress distribution induced in the crystals evidently affects the E_2 phonon frequency. This behaviour agrees with XRD results discussed in Section 3.1, for the ZnO@ZnS (water) Raman peaks are located at 346 and 379 cm^{-1}, which corresponds accurately to the first order TO and LO phonon modes in ZnS, respectively [34]. The vibrational peaks of ZnO@ZnS (EG) core–shell, after the sulfuration process are in agreement of Raman modes of ZnS which give further evidence that ZnO was clearly decorated with ZnS when EG solvent is used in (Fig. 3B).

3.4. Optical study

The ZnO, and ZnO@ZnS optical properties were measured using UV–vis diffuse reflection methodology. The band gap energies (E_g) of ZnO@ZnS core–shell system was estimated from the graph of $(\alpha h\nu)^2$ versus $h\nu$ (Tauc plot), as seen in (Fig. 4A,B). The absorption coefficient α that is related to the band gap E_g as $(\alpha h\nu)^2 = k(h\nu E_g)$, where $h\nu$ is the incident light energy and k is a constant.

Fig. 4A. shows the absorption for the ZnO (H_2O), ZnO@ZnS (H_2O) and ZnS (H_2O). The optical band gap of ZnO (H_2O) is 3.0 eV and as can be seen it's smaller than the band gap of the bulk ZnO [35]. The possible reason could be due to electronic and structural defects arising during the MAS synthesis. This same behaviour was already observed for other compounds in a previous work using the same synthesis methodology [28]. This band gap reduction can improve

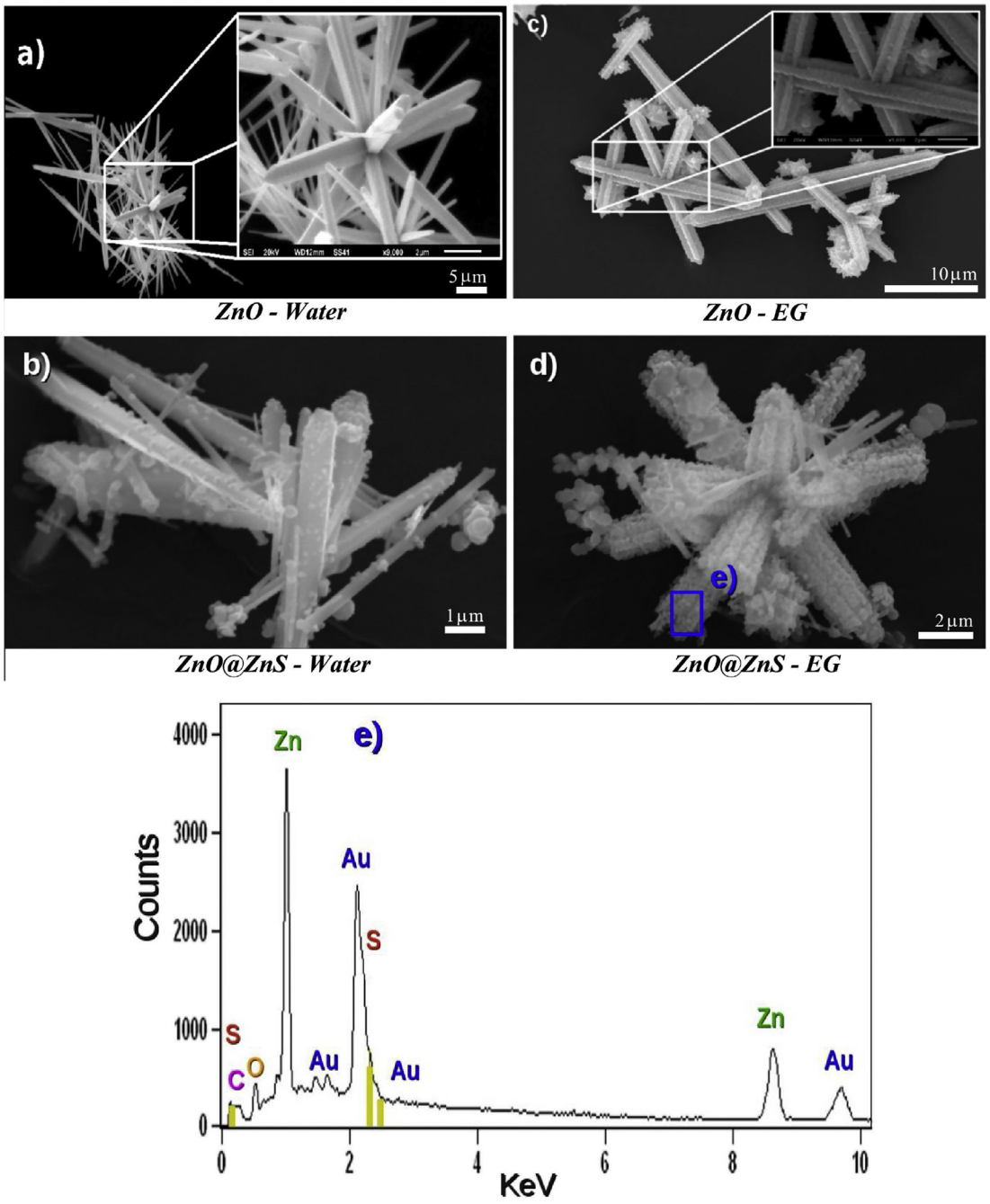

Fig. 2. FE-SEM images and EDX analysis of crystals synthesized by MAS method a) ZnO–H_2O, b) ZnO@ZnS–H_2O, c) ZnO-EG, d) ZnO@ZnS-EG, e) EDX (5 kV of ZnO@ZnSr-EG) analysis.

the light absorption of ZnO at visible range, favouring solar-cells applications.

The decoration process of ZnO (H_2O) with ZnS (H_2O) leads to reduction of the optical band gap to ≈2.9 eV. This behaviour is not really conclusive, because even though UV–vis measurements are made several times, 0.1 eV can be include as measurement haziness. Also, the ZnS band gap of 3.1 eV indicates that the decorating was not highly effective in water medium. The reduction on ZnS (H_2O) band gap in relation to ZnS obtained using EG is due to the different structural distortions produced by EG and water as a result of water be ionic solvent and EG not. Another important aspect is the less sharp and the expressive absorption tail of ZnS which are responsible by the wide range absorptions.

On the other hand, in Fig. 4B, the obtained band gap were respectively 3.1 and 3.7 eV for pure ZnO (EG) and ZnS (EG). The ZnO@ZnS (EG) decorated system has two absorption bands at 3.1 eV and at 3.5 eV which correspond to the ZnO (EG) and ZnS (EG) phases, respectively. The double band gap regime allows two absorptions at different electromagnetic ranges increasing the absorptions efficiency and hence enabling solar cell application, specially for solar cells with high efficiency close to ultraviolet region.

These results clearly show that the best decoration of ZnO with ZnS was using EG as solvent which was already noted in previous XRD and Raman datas. Furthermore, the formation of ZnS shell over the core ZnO, leads ZnO@ZnS to type-II band alignment through the

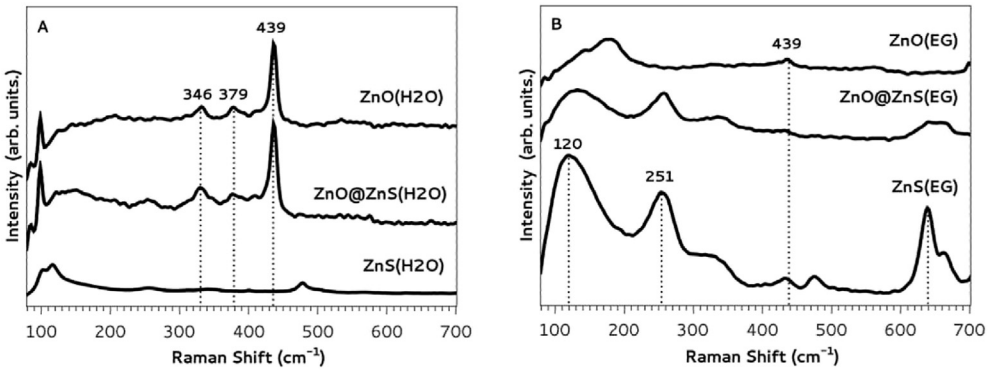

Fig. 3. Raman spectroscopy core–shell and individual samples synthesized by A) H_2O, B) EG.

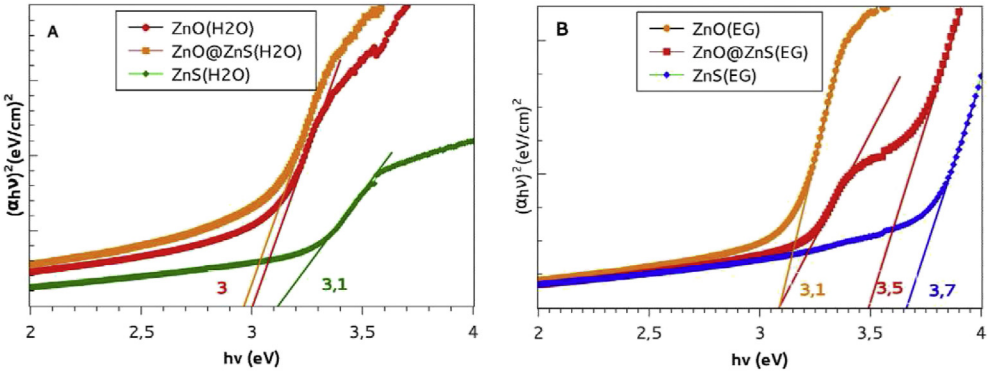

Fig. 4. UV–vis absorption of ZnO, ZnS and ZnO@ZnS for $(\alpha h\nu)^2$ versus $h\nu$ (A) H_2O and (B) EG.

induction of charge separation at the interface of the two different materials. Thus, the electrons and holes are localized in different regions of the ZnO@ZnS core–shell and this reduces the chance of recombination of the charge carriers. The type-II band alignment also forms appropriate conduction band edge lines to facilitate electron transfer [36].

Using photoluminescence (PL) spectroscopy is noticeable that the observed PL emission in Fig. 5A is broad and cover almost all the visible range centered at 530 nm for pure ZnO (H_2O). This is called green-yellow band for visible luminescence or deep level emission (DLE) [37], which is due to the discrete deep energy levels into the band gap formed by the point defects [38]. The ZnO@ZnS samples demonstrate the same qualitative character of luminescence. However, the peak shifts slightly towards lower energies and located at 580 nm. This behaviour could be expected for type-II band alignment [39] that originates from the electron–hole recombination at the interface [40].

Samples synthesized with EG solvent are shown in Fig. 5B. The ZnO peak is slightly shifted towards lower energies with main emission located at 580 nm, while for ZnS and the ZnO@ZnS samples the emissions become too weak. The qualitative character of luminescence for ZnO@ZnS reports two peaks located at 400 nm and 530 nm. These two peaks appear due to the high decoration of ZnO by ZnS using EG as solvent, in agreement with UV–vis absorption and Raman results. Besides, the sharp peak at 400 nm can be attributed to the band alignment, allowing the inter bands exciton annihilation by means of photon emission. Moreover, this emission is too weak indicating that this is a non-relevant process.

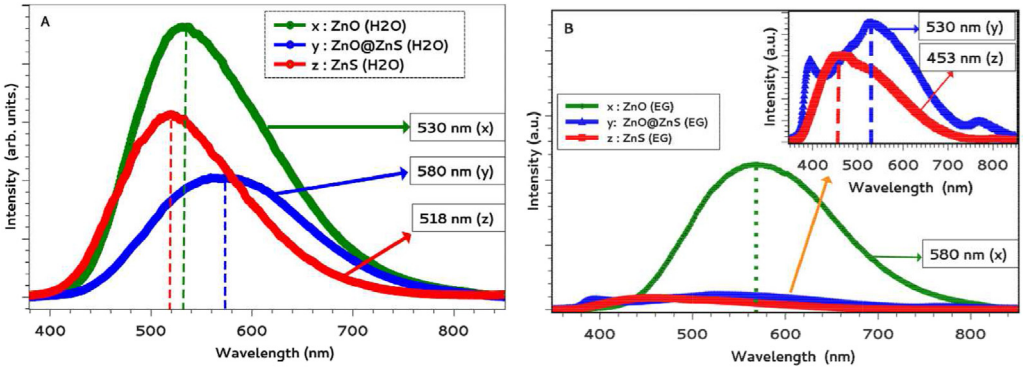

Fig. 5. Photoluminescence spectra of the ZnO and ZnO@ZnS core–shell in A) H_2O; B) Inset is a zoom of the PL spectra of ZnO (EG) and ZnO@ZnS (EG).

Nevertheless, the luminescence efficiency of ZnO@ZnS also set forth the strong dependence of decorations. This effect is noticeable in Fig. 5B which the luminescence emission of decorated system has about the same intensity of ZnS samples.

3.5. Type-II band alignment

The construction of a reliable band alignment from both theory and experiment has thus been a long-standing issue because of its fundamental and technological importance [41].

Historically, various theories have been proposed in connection with the band alignment of semiconductors, particularly, for group II-VI semiconductors with wide band gap, ZB structure (ZnS) and WZ structure (ZnO). Especially the origin of band alignment in ZnO@ZnS is still controversial due to synthesis methods as MAS used in this work. Comparing to the core ZnO, the fabricated ZnO@ZnS exhibit enhanced red-shift emission and present type-II band alignment [42]. Recently, ZnO/ZnS heterostructures have attracted theoretical and experimental interest for showing superior optoelectronic properties to their individual materials due to their type-II band alignment that was detected according to the (Fig. 5) for ZnO@ZnS (H_2O). In type-II systems, the shell growth causes a red-shift of the emission wavelength of the core and leads to a smaller effective band gap (Fig. 4). Additionally, the ZnO@ZnS samples synthesized in EG also denotes the type-II band alignment as was described in UV-is results and confirmed in PL results by strong reduction of PL emission associated to red-shift. It is important highlight that ZnO@ZnS (EG) report a more evident type-II band alignment effect. Than we can claim that the type-II band alignment are present in both systems, moreover if the objective is specially solar cells with high efficiency close to ultraviolet region the ZnO@ZnS (EG) can be potentially more useful.

4. Conclusions

In summary, ZnO and ZnO@ZnS (water or EG) core–shell system was prepared by an efficient MAS method. Their structural and photonic properties were investigated in detail. FE-SEM images and the XRD patterns analysis confirmed a clear relationship between the nature of the solvent used and its effective or non-effective decorations. Also was demonstrated that ZnO multi-wires are not dependent of solvent (water or EG) used in our synthesis. Optical characterization using UV–visible and PL spectroscopy allow the demonstration a clear dependence of photonic features with different solvents (water or EG). The results clearly show that the decoration with the solvent EG was better than water. On the other hand, the formation of a ZnS shell around core ZnO nanorod results in a type-II band alignment for ZnO@ZnS synthesized in water medium. Therefore, synthesis method used prove the ability to control the properties of the material decoration through the changes on the synthesis parameters. Thereby it is also possible to control the absorption and photon emissions.

Acknowledgements

The authors are grateful by financial support of the Brazilian research funding institution FAPESP (2009/17752-0), FAPERGS (2031-2551/13-9SIAS) and CNPq (MCT/CNPq 458452/2014-9). Also acknowledge CEME-Sul in Federal University of Rio Grande by Technical support by user felicities of MEV and X ray diffraction.

References

[1] P. Reiss, M. Protiere, L. Li, Core/shell semiconductor nanocrystals, small 5 (2009) 154–168.
[2] C. de Mello Donegá, Synthesis and properties of colloidal heteronanocrystals, Chem. Soc. Rev. 40 (2011) 1512–1546.
[3] T. Pisanic Ii, Y. Zhang, T. Wang, Quantum dots in diagnostics and detection: principles and paradigms, Analyst 139 (2014) 2968–2981.
[4] Z.L. Wang, Nanostructures of zinc oxide, Mater. Today 7 (2004) 26–33.
[5] S.S. Kumar, P. Venkateswarlu, V.R. Rao, G.N. Rao, Synthesis, characterization and optical properties of zinc oxide nanoparticles, Int. Nano Lett. 3 (2013) 1–6.
[6] W.D. Zhou, X. Wu, Y.C. Zhang, M. Zhang, Solvothermal synthesis of hexagonal ZnO nanorods and their photoluminescence properties, Mater. Lett. 61 (2007) 2054–2057.
[7] Y.-C. Chen, H.-Y. Cheng, C.-F. Yang, Y.-T. Hsieh, Investigation of the optimal parameters in hydrothermal method for the synthesis of ZnO nanorods, J. Nanomater. (2014).
[8] A. Al-Kahlout, Thermal treatment optimization of ZnO nanoparticles-photoelectrodes for high photovoltaic performance of dye-sensitized solar cells, J. Assoc. Arab Univ. Basic Appl. Sci. (2014).
[9] K. Tam, C. Cheung, Y. Leung, A. Djurišic, C. Ling, C. Beling, S. Fung, W. Kwok, W. Chan, D. Phillips, et al., Defects in ZnO nanorods prepared by a hydrothermal method, J. Phys. Chem. B 110 (2006) 20865–20871.
[10] R. Li, J. Che, H. Zhang, J. He, A. Bahi, F. Ko, Study on synthesis of ZnO nanorods and its uv-blocking properties on cotton fabrics coated with the ZnO quantum dot, J. Nanoparticle Res. 16 (2014) 1–12.
[11] A. Janotti, C.G. Van de Walle, Oxygen vacancies in ZnO, Appl. Phys. Lett. 87 (2005) 122102.
[12] C. Wang, D. Wu, P. Wang, Y. Ao, J. Hou, J. Qian, Effect of oxygen vacancy on enhanced photocatalytic activity of reduced ZnO nanorod arrays, Appl. Surf. Sci. 325 (2015) 112–116.
[13] P. Srinivasan, B. Subramanian, Y. Djaoued, J. Robichaud, T. Sharma, R. Bruning, Facile synthesis of mesoporous nanocrystalline ZnO bipyramids and spheres: characterization, and photocatalytic activity, Mater. Chem. Phys. 155 (2015) 162–170.
[14] A. Kole, P. Kumbhakar, T. Ganguly, Observations of unusual temperature dependent photoluminescence anti-quenching in two-dimensional nanosheets of ZnS/ZnO composites and polarization dependent photoluminescence enhancement in fungi-like ZnO nanostructures, J. Appl. Phys. 115 (2014) 224306.
[15] O. Chen, Y. Yang, T. Wang, H. Wu, C. Niu, J. Yang, Y.C. Cao, Surface-functionalization-dependent optical properties of ii–vi semiconductor nanocrystals, J. Am. Chem. Soc. 133 (2011) 17504–17512.
[16] A. Brayek, M. Ghoul, A. Souissi, I.B. Assaker, H. Lecoq, S. Nowak, S. Chaguetmi, S. Ammar, M. Oueslati, R. Chtourou, Structural and optical properties of ZnS/ZnO core/shell nanowires grown on ITO glass, Mater. Lett. 129 (2014) 142–145.
[17] T. Ghrib, M. Abdullah Al-Messiere, A. Lafi Al-Otaibi, Synthesis and characterization of ZnO/ZnS core/shell nanowires, J. Nanomater. (2014).
[18] Z. Wang, J. Wang, T.-K. Sham, S. Yang, Origin of luminescence from ZnO/cds core/shell nanowire arrays, Nanoscale 6 (2014) 9783–9790.
[19] C.W. Raubach, Y.V. De Santana, M.M. Ferrer, P.G. Buzolin, J.R. Sambrano, E. Longo, Photocatalytic activity of semiconductor sulfide heterostructures, Dalton Trans. 42 (2013) 11111–11116.
[20] P. Guo, J. Jiang, S. Shen, L. Guo, ZnS/ZnO heterojunction as photoelectrode: type ii band alignment towards enhanced photoelectrochemical performance, Int. J. Hydrogen Energy 38 (2013) 13097–13103.
[21] M. Sookhakian, Y. Amin, W. Basirun, M. Tajabadi, N. Kamarulzaman, Synthesis, structural, and optical properties of type-ii ZnO–ZnS core–shell nanostructure, J. Luminescence 145 (2014) 244–252.
[22] Y.-Z. Zheng, H. Ding, Y. Liu, X. Tao, G. Cao, J.-F. Chen, In situ hydrothermal growth of hierarchical ZnO nanourchin for high-efficiency dye-sensitized solar cells, J. Power Sources 254 (2014) 153–160.
[23] L. Yu, W. Chen, D. Li, J. Wang, Y. Shao, M. He, P. Wang, X. Zheng, Inhibition of photocorrosion and photoactivity enhancement for ZnO via specific hollow ZnO core/ZnS shell structure, Appl. Catal. B Environ. 164 (2015) 453–461.
[24] W. Xitao, L. Rong, W. Kang, Synthesis of ZnO@ZnS-bi2s3 core-shell nanorod grown on reduced graphene oxide sheets and its enhanced photocatalytic performance, J. Mater. Chem. A 2 (2014) 8304–8313.
[25] J. Rouhi, C.R. Ooi, S. Mahmud, M.R. Mahmood, Facile synthesis of vertically aligned cone-shaped ZnO/ZnS core/shell arrays using the two-step aqueous solution approach, Mater. Lett. 147 (2015a) 34–37.
[26] J. Rouhi, M.H. Mamat, C.R. Ooi, S. Mahmud, M.R. Mahmood, High-performance dye-sensitized solar cells based on morphology-controllable synthesis of ZnO–ZnS heterostructure nanocone photoanodes, PloS One 10 (2015b).
[27] S.I.U. Shah, A.L. Hector, X. Li, J.R. Owen, Solvothermal synthesis and electrochemical charge storage assessment of Mn_3N_2, J. Mater. Chem. A (2015).
[28] R.U. Fassbender, T.S. Lilge, S. Cava, J. Andrés, L.F. da Silva, V.R. Mastelaro, E. Longo, M.L. Moreira, Fingerprints of short-range and long-range structure in $bazr_{1-x}hf_xO_3$ solid solutions: an experimental and theoretical study, Phys. Chem. Chem. Phys. 17 (2015) 11341–11349.
[29] A. De Moura, R. Lima, M. Moreira, D. Volanti, J. Espinosa, M. Orlandi, P. Pizani, J.A. Varela, E. Longo, ZnO architectures synthesized by a microwave-assisted hydrothermal method and their photoluminescence properties, Solid State Ionics 181 (2010) 775–780.
[30] C.W. Raubach, L. Polastro, M.M. Ferrer, A. Perrin, C. Perrin, A.R. Albuquerque, P.G. Buzolin, J.R. Sambrano, Y.B. de Santana, J.A. Varela, et al., Influence of solvent on the morphology and photocatalytic properties of ZnS decorated

CeO_2 nanoparticles, J. Appl. Phys. 115 (2014) 213514.
[31] M. Bitenc, M. Marinšek, Z.C. Orel, Preparation and characterization of zinc hydroxide carbonate and porous zinc oxide particles, J. Eur. Ceram. Soc. 28 (2008) 2915–2921.
[32] R. Ahmad, N. Tripathy, N.K. Jang, G. Khang, Y.-B. Hahn, Fabrication of highly sensitive uric acid biosensor based on directly grown ZnO nanosheets on electrode surface, Sensors Actuators B Chem. 206 (2015) 146–151.
[33] Y.-W. Tseng, F.-Y. Hung, T.-S. Lui, S.-J. Chang, Structural and raman properties of silver-doped ZnO nanorod arrays using electrically induced crystallization process, Mater. Res. Bull. 64 (2015) 274–278.
[34] G. Shen, D. Chen, C.J. Lee, Hierarchical saw-like ZnO nanobelt/ZnS nanowire heterostructures induced by polar surfaces, J. Phys. Chem. B 110 (2006) 15689–15693.
[35] A. Kushwaha, M. Aslam, ZnS shielded ZnO nanowire photoanodes for efficient water splitting, Electrochim. Acta 130 (2014) 222–231.
[36] Y. Wang, X. Zhan, F. Wang, Q. Wang, M. Safdar, J. He, Crystalline ZnO/ZnS_xSe_{1-x} core–shell nanowire arrays for efficient visible-light photoelectrocatalysis, J. Mater. Chem. A 2 (2014) 18413–18419.
[37] Y. Lei, F. Qu, X. Wu, Assembling ZnO nanorods into microflowers through a facile solution strategy: morphology control and cathodoluminescence properties, Nano–Micro Lett. 4 (2012) 45–51.
[38] P. Chen, L. Gu, X. Cao, From single ZnO multipods to heterostructured ZnO/ZnS, ZnO/ZnSe, ZnO/Bi_2S_3 and ZnO/Cu_2S multipods: controlled synthesis and tunable optical and photoelectrochemical properties, CrystEngComm 12 (2010) 3950–3958.
[39] S. Zhang, B. Yin, H. Jiang, F. Qu, A. Umar, X. Wu, Hybrid ZnO/ZnS nanoforests as the electrode materials for high performance supercapacitor application, Dalton Trans. 44 (2015) 2409–2415.
[40] R. Zamiri, D.M. Tobaldi, H.A. Ahangar, A. Rebelo, M.P. Seabra, M.S. Belsley, J.M.F. Ferreira, Study of far infrared optical properties and, photocatalytic activity of ZnO/ZnS hetero-nanocomposite structure, RSC Adv. 4 (2014) 35383–35389.
[41] Y. Hinuma, A. Grüneis, G. Kresse, F. Oba, Band alignment of semiconductors from density-functional theory and many-body perturbation theory, Phys. Rev. B 90 (2014) 155405.
[42] A. Sadollahkhani, O. Nur, M. Willander, I. Kazeminezhad, V. Khranovskyy, M. Eriksson, R. Yakimova, P.-O. Holtz, A detailed optical investigation of ZnO@ZnS core–shell nanoparticles and their photocatalytic activity at different ph values, Ceram. Int. 41 (2015) 7174–7184.